

A new mathematical approach to finding global solutions of the magnetic structure determination problem

| | |
|------------------------------|---|
| 著者 | Tomiyasu K., Oishi-Tomiyasu R., Matsuda M., Matsuhira K. |
| journal or publication title | Scientific Reports |
| volume | 8 |
| page range | 16228-1-16228-8 |
| year | 2018-11-01 |
| その他のタイトル | A New Mathematical Approach to Finding Global Solutions of The Magnetic Structure Determination Problem |
| URL | http://hdl.handle.net/10228/00007298 |

doi: info:doi/10.1038/s41598-018-34443-2

SCIENTIFIC REPORTS

OPEN

A new mathematical approach to finding global solutions of the magnetic structure determination problem

K. Tomiyasu¹, R. Oishi-Tomiyasu^{2,3}, M. Matsuda⁴ & K. Matsuhira⁵

Determination of magnetic structure is an important analytical procedure utilized in various fields ranging from fundamental condensed-matter physics and chemistry to advanced manufacturing. It is typically performed using a neutron diffraction technique; however, finding global solutions of the magnetic structure optimization problem represents a significant challenge. Generally, it is not possible to mathematically prove that the obtained magnetic structure is a truly global solution and that no solution exists when no acceptable structure is found. In this study, the global optimization technique called semidefinite relaxation of quadratic optimization, which has attracted much interest in the field of applied mathematics, is proposed to use as a new analytical method for the determination of magnetic structure, followed by the application of polarized neutron diffraction data. This mathematical approach allows avoiding spurious local solutions, decreasing the amount of time required to find a tentative solution and finding multiple solutions when they exist.

Development of method for determining crystal and magnetic structure is an important issue^{1–3}. The magnetic structure of a compound is directly related to the microscopic origins of various intriguing magnetic phenomena observed in physics, chemistry, biology and geology^{4–11}. Accurate information on the experimentally determined magnetic structures can be potentially used to effectively design functional materials and opens multiple opportunities for utilizing advanced first-principle calculations and informatics approaches. Furthermore, the responses of the analysed magnetic structure to external factors such as temperature, pressure, electromagnetic field, light and environment are usually related to the corresponding changes in the macroscopic properties of minerals and biomolecules.

Since the pioneering work of Shull *et al.* published in 1951¹, many studies on the determination of the magnetic structures of various materials by neutron diffraction have been performed. Thus, Izyumov, Kovalev and Bertaut developed the irreducible representation (IR) theory, which successfully classified magnetic structures by their magnetic point symmetries obtained through the analysis of neutron diffraction data^{12–14}. Moreover, the modern neutron diffractometers exhibit relatively high statistical accuracy and resolution^{15,16}. However, analysing neutron diffraction data to determine the correct magnetic structure represents a challenging task. The major issue here is the existence of so-called local solutions to the optimization problem (Fig. 1A). The analysis procedure is mathematically categorized as the nonlinear optimization, in which the obtained diffraction data points are fitted with the function of neutron scattering cross-section characterized by high-dimensional nonlinear parameters such as magnetic moment vectors¹⁷. After performing nonlinear optimization, it is very difficult to prove that the best solution obtained via various numerical models is the global one. Furthermore, multiple or many solutions are hidden in some cases, and no solutions exist in other cases. To mitigate these issues, global optimization techniques including a simulated annealing method, the Monte Carlo method and genetic algorithms can be used^{18–23}. However, none of these approaches can determine the global solution(s) with 100% probability.

¹Department of Physics, Tohoku University, Aoba, Sendai, 980-8578, Japan. ²Faculty of Science, Yamagata University, Yamagata, 990-8560, Japan. ³JST, PRESTO, Saitama, 332-0012, Japan. ⁴Neutron Scattering Division, Oak Ridge National Laboratory, Oak Ridge, TN, 37831, USA. ⁵Faculty of Engineering, Kyusyu Institute of Technology, Kitakyusyu, 804-8550, Japan. Correspondence and requests for materials should be addressed to K.T. (email: tomiyasu@tohoku.ac.jp) or R.O.-T. (email: ryoko_tomiyasu@sci.kj.yamagata-u.ac.jp)

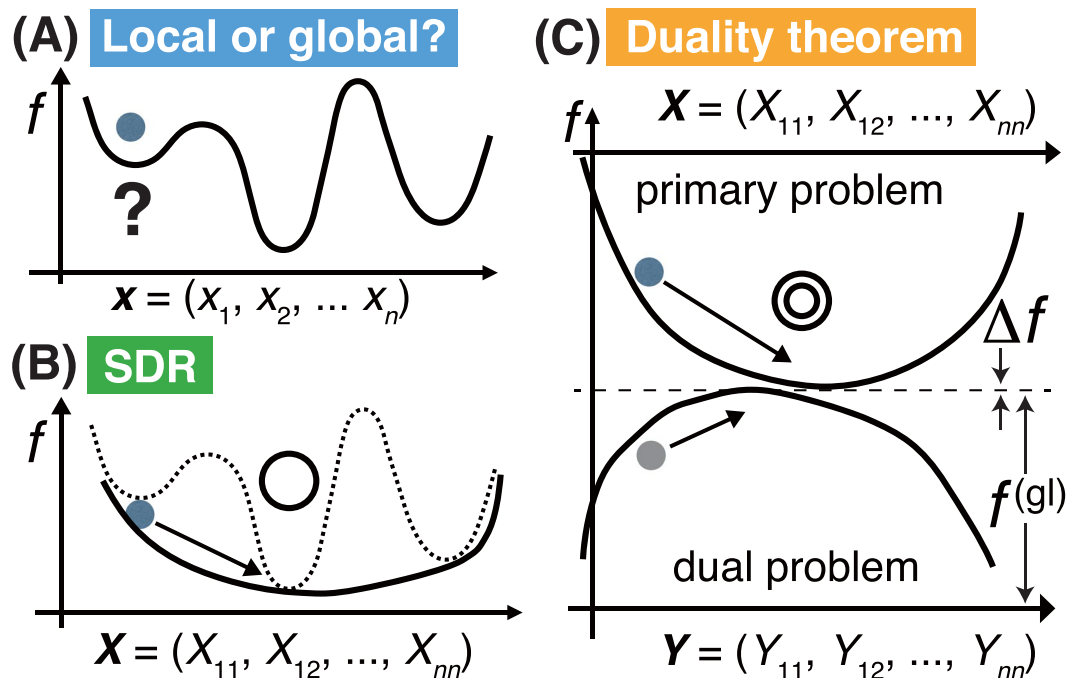


Figure 1. Schematic diagrams illustrating the non-linear optimization process. (A) Before relaxation. (B) SDR technique. (C) Duality theorem combined with SDR. The objective function f is globally minimized to the global optimum value $f^{(gl)}$. When the duality gap Δf is close to zero (corresponding to the square root of the machine epsilon), the global optimization process is complete according to the duality theorem. In panels (B) and (C), the solid balls represent the paths toward feasible solutions chosen by the interior point method.

In this study, a new analytical method for the determination of magnetic structure is proposed, which allows (i) judging whether the obtained solution is a truly global one; (ii) evaluating the uniqueness of the solution obtained for a given set of experimental data; and (iii) completing the global optimization procedure in a very short time (typically, less than several seconds). Furthermore, the applicability of the proposed method is demonstrated using polarized-neutron powder diffraction data.

Mathematical Formulation for Applications of Semidefinite Relaxation Method

Relaxation techniques have been previously developed in the field of mathematical programming. In particular, semidefinite relaxation (SDR) combined with semidefinite programming (SDP) has found many applications in applied mathematics and engineering (for example, see Chapter 2.2 in ref.²⁴). SDR is an efficient technique for solving nonlinear optimization problems, such as quadratic programs (QPs), namely the minimization of multivariate quadratic polynomials under constraints. It should be noted that SDR could provide both fast convergence and a numerical proof of the global optimality of the obtained solutions using the global convergence property and duality theorem of the convex programming methods, as schematically shown in Fig. 1(B,C).

In the field of optical imaging, Candès *et al.* published a pioneering work (called the PhaseLift method), in which a sparse modelling approach was adopted for general phase retrieval²⁵. Furthermore, one of the authors (ROT) developed an SDR-based mathematical approach to investigate whether a crystal structure could be uniquely identified using only diffraction data and independent atomic model²⁶.

In this study, this method was applied to magnetic structure analysis by replacing the optimized parameters with magnetic moments. The problem of magnetic structure determination can be mathematically described by the following set of N quadratic equations:

$$I_{\text{mag,obs}}(Q_k) \approx I_{\text{mag,cal}}(Q_k) = \mathbf{x}^T S_k \mathbf{x} = \sum_{1 \leq i, j \leq n} S_k(i, j) x_i x_j \quad (1 \leq k \leq N), \quad (1)$$

where $I_{\text{mag,obs}}(Q_k)$ and $I_{\text{mag,cal}}(Q_k)$ denote the observed and calculated integrated magnetic diffraction intensities at the magnetic reflection $Q_k = h_{\text{mag}} k_{\text{mag}} l_{\text{mag}}$, respectively; $\mathbf{x} = (x_1, \dots, x_n)^T$ and S_k represents the coefficient matrix numerically obtained using the scattering cross-section formula for each Q_k , which consists of the absolute intensity scale factor, magnetic form factor, Lorentz factor, multiplicity and structural weight factor (the details of this formula are summarized in Supplementary Information).

The symbol \approx indicates that each $I_{\text{mag,obs}}(Q_k)$ value includes an experimental error. In order to incorporate all errors, the following optimization problem is solved:

$$\begin{cases} \text{Minimize } \sum_{k=1}^N \frac{|I_{\text{mag,obs}}(Q_k) - \mathbf{x}^T \mathbf{S}_k \mathbf{x}|}{\text{Err}[I_{\text{mag,obs}}(Q_k)]}, \\ \text{subject to: } |x_i| \leq R_i (1 \leq i \leq n). \end{cases} \quad (2)$$

The inequality $|x_i| \leq R_i$ can be also removed if the permitted range of $|x_i|$ (R_i , for example, the upper limit of magnetic moment) is uncertain while maintaining the validity of the subsequent discussion of the SDR and SDP techniques.

Equation (2) is classified as a so-called l^1 -norm minimization problem, which is equivalent to the following form of the quadratic programming problem:

$$\begin{cases} \text{Minimize } \sum_{k=1}^N \frac{\eta_k^+ + \eta_k^-}{2}, \\ \text{subject to: } \frac{I_{\text{mag,obs}}(Q_k) - \mathbf{x}^T \mathbf{S}_k \mathbf{x}}{\text{Err}[I_{\text{mag,obs}}(Q_k)]} = \frac{\eta_k^+ - \eta_k^-}{2} (1 \leq k \leq N), \\ x_i^2 + y_i = R_i^2, y_i \geq 0 (1 \leq i \leq n), \\ \eta_k^+ \geq 0, \eta_k^- \geq 0 (1 \leq k \leq N). \end{cases} \quad (3)$$

The problems described by equations (2) and (3) are equivalent since they have the same set of solutions \mathbf{x} and the minimized values of the objective functions (more details are provided in Supplementary Information). The basic strategy utilized in this work is to apply SDR to equation (3) in order to solve equation (2) and then provide a computational proof on the global convergence property of the solution. The least-squares minimization of the $\sum_{k=1}^N \left[\frac{I_{\text{mag,obs}}(Q_k) - \mathbf{x}^T \mathbf{S}_k \mathbf{x}}{\text{Err}[I_{\text{mag,obs}}(Q_k)]} \right]^2$ function is avoided because a small increase in the polynomial degree considerably magnifies the size of the SDR problem (it increases proportionally to the power of N). Thus, it is possible to locate the global optimum by performing l^1 -norm minimization, which can be subsequently used as the initial parameter of the normal least-squares method to calculate the refined parameters and then compare them with literature data.

Application to Experimental Data Analysis

Experimental results. The developed SDR method was verified by applying it to the experimental data obtained for pyrochlore $\text{Nd}_2\text{Ir}_2\text{O}_7$, which served as a proximate material for a three-dimensional Weyl semimetal and a component of spintronic devices on the basis of its geometrically frustrated magnetism and $5d$ -electron configuration^{27–32}. This state theoretically corresponds to the all-in-all-out type of magnetic structure described by the magnetic propagation vector $\mathbf{k}_{\text{mag}} = (0, 0, 0)$, in which all the magnetic moments are oriented either towards the centre of the participating tetrahedron or in the opposite direction^{30,32}. This prediction was experimentally confirmed in previous unpolarized neutron diffraction studies^{33,34}. However, the superposition of the nuclear and magnetic reflections observed for the magnetic structures with $\mathbf{k}_{\text{mag}} = (0, 0, 0)$ produces ambiguous results during their separation. Furthermore, it is not possible to mathematically prove with 100% certainty the absence of other acceptable solutions to the problem of magnetic structure determination. Thus, in this work, polarized neutron diffraction studies were performed for this material, and the obtained magnetic structure was verified mathematically.

Figure 2 shows the representative neutron diffraction data obtained for $\text{Nd}_2\text{Ir}_2\text{O}_7$ at the minimum temperature $T = 1.4$ K. The non-spin-flip and spin-flip parameters I_{OFF} and I_{ON} roughly correspond to the nuclear and magnetic reflection components I_{nuc} and I_{mag} , respectively. The magnitude of I_{OFF} is systematically larger than I_{ON} at all temperatures, thus confirming the necessity of conducting polarized neutron diffraction experiments. For I_{ON} , the intensity of the 113 reflection increases with decreasing temperature, indicating the existence of strong temperature dependence for this reflection, which is not observed for the 222 reflection. Moreover, as the flipping ratio of the neutron beam in the actual experiments is finite, the magnitudes of I_{ON} and I_{OFF} can be expressed by the following formulas:

$$\begin{cases} I_{\text{OFF}} = (1 - r_{\text{mix}})I_{\text{nuc}} + r_{\text{mix}}I_{\text{mag}}, \\ I_{\text{ON}} = r_{\text{mix}}I_{\text{nuc}} + (1 - r_{\text{mix}})I_{\text{mag}}, \end{cases}$$

where $r_{\text{mix}} = N_- / (N_+ + N_-)$ is the mixing rate, and N_+ (N_-) denotes the number of majority-spin (minority-spin) neutrons. The value of r_{mix} is selected to satisfy the condition $I_{\text{mag}} = 0$; hence, $I_{\text{ON}} = r_{\text{mix}}I_{\text{nuc}}$ at the paramagnetic $T = 40$ K. As a result, the pure magnetic intensity I_{mag} can be determined by combining I_{OFF} and I_{ON} . A more detailed explanation and data obtained for other reflections are presented in Supplementary Information, while the calculated $I_{\text{mag,obs}}$ values are listed in Table 1.

Magnetic structure analysis results. The arbitrary magnetic structure with $\mathbf{k}_{\text{mag}} = (0, 0, 0)$ in the space group $Fd\bar{3}m$ is described as the function of $\mathbf{x}_{\text{arb}} = (m^{(\text{Nd})}_1, \dots, m^{(\text{Nd})}_{12}, m^{(\text{Ir})}_1, \dots, m^{(\text{Ir})}_{12})$ containing $n_{\text{arb}} = 24$ variables generated by the eight magnetic atoms of the unit cell and three Cartesian coordinates. Here, the magnetic symmetry was classified by performing IR analysis (this procedure is generally not required for the proposed method; however, it may be potentially useful because of the reduction of the number of variables if the number of observed reflection points is limited). The possible magnetic structures are described by the representations

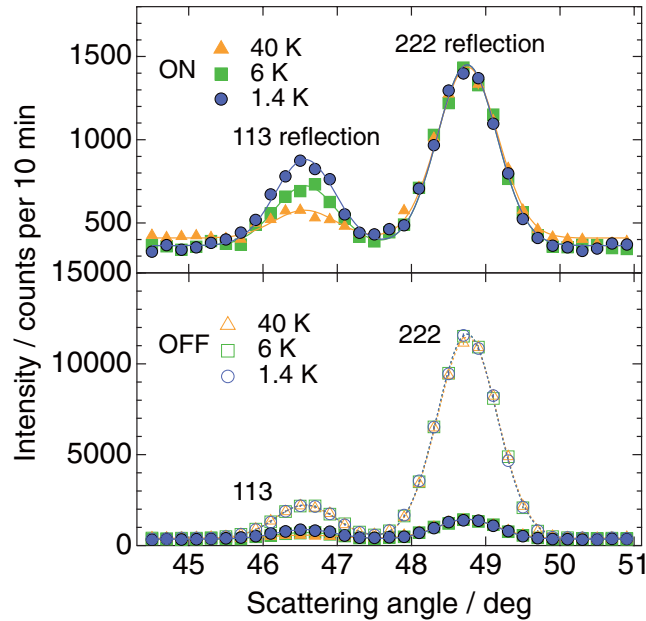


Figure 2. Typical polarized neutron diffraction data obtained for pyrochlore $\text{Nd}_2\text{Ir}_2\text{O}_7$. ON/OFF denotes the spin-flip/non-spin-flip scattering channel. The lower panel displays both the overall OFF and ON data, whereas the upper panel depicts the low-intensity ON data at a higher magnification. The solid and dotted curves show the results of Gaussian fitting.

| $h_{\text{mag}} k_{\text{mag}} l_{\text{mag}}$ | $I_{\text{mag,obs}} (1.4 \text{ K})$ | $I_{\text{mag,cal},\Gamma_3}$ | $I_{\text{mag,cal},\Gamma_5}$ | $I_{\text{mag,cal},\Gamma_7}$ | $I_{\text{mag,cal},\Gamma_9}$ |
|--|--------------------------------------|-------------------------------|-------------------------------|-------------------------------|-------------------------------|
| 111 | 0 ± 53 | 0 | 7 | 0 | 457 |
| 200 | 0 ± 36 | 0 | 0 | 0 | 1 |
| 220 | 932 ± 54 | 932 | 932 | 0 | 1 |
| 113 | 1796 ± 68 | 1795 | 4 | 0 | 860 |
| 222 | 0 ± 63 | 0 | 0 | 0 | 0 |
| 400 | 0 ± 37 | 0 | 0 | 0 | 0 |
| 331 | 349 ± 54 | 580 | 5 | 0 | 349 |
| 420 | 884 ± 62 | 588 | 541 | 0 | 2 |

Table 1. Experimentally observed and calculated integrated magnetic scattering intensities. The symbol \pm denotes the experimental errors.

$\Gamma_{\text{Nd}} = \Gamma_3 + 2\Gamma_5 + 3\Gamma_7 + 6\Gamma_9$ and $\Gamma_{\text{Ir}} = \Gamma_3 + 2\Gamma_5 + 3\Gamma_7 + 6\Gamma_9$, where Γ_3 corresponds to the all-in all-out type of the magnetic structure, and the coefficients denote the numbers of basis vectors summarized in Table 2^{18,35}. Hence, the total numbers of variables are reduced to $n_{\Gamma_3} = 2$, $n_{\Gamma_5} = 4$, $n_{\Gamma_7} = 6$ and $n_{\Gamma_9} = 12$. Furthermore, representation Γ_9 includes six ferromagnetic basis vectors. However, the $\text{Nd}_2\text{Ir}_2\text{O}_7$ structure exhibits only extremely weak spontaneous magnetization (around $10^{-4} \mu_B/\text{formula unit}$)²⁹, which is significantly below the detection limit of the neutron diffraction technique. Therefore, the ferromagnetic basis vectors are precluded and the value of n_{Γ_9} is further reduced from 12 to 6 during the analysis of the neutron diffraction data.

Thus, the variables used for the magnetic structure analysis in this work are defined as follows: $\mathbf{x}_{\Gamma_3} = (m^{(\Gamma_3, \text{Nd})_1}, m^{(\Gamma_3, \text{Ir})_1})$, $\mathbf{x}_{\Gamma_5} = (m^{(\Gamma_5, \text{Nd})_1}, m^{(\Gamma_5, \text{Nd})_2}, m^{(\Gamma_5, \text{Ir})_1}, m^{(\Gamma_5, \text{Ir})_2})$, $\mathbf{x}_{\Gamma_7} = (m^{(\Gamma_7, \text{Nd})_1}, m^{(\Gamma_7, \text{Nd})_2}, m^{(\Gamma_7, \text{Nd})_3}, m^{(\Gamma_7, \text{Ir})_1}, m^{(\Gamma_7, \text{Ir})_2}, m^{(\Gamma_7, \text{Ir})_3})$ and $\mathbf{x}_{\Gamma_9} = (m^{(\Gamma_9, \text{Nd})_1}, m^{(\Gamma_9, \text{Nd})_2}, m^{(\Gamma_9, \text{Nd})_3}, m^{(\Gamma_9, \text{Ir})_1}, m^{(\Gamma_9, \text{Ir})_2}, m^{(\Gamma_9, \text{Ir})_3})$. The goal is to determine the globally optimal solutions \mathbf{x} for representations Γ_3 , Γ_5 , Γ_7 and Γ_9 using the $I_{\text{mag,obs}}$ magnitudes listed in Table 1. After that, the solution characterized by the best fit can be selected.

The output values produced by the SDP solver are as follows.

- (1) The convergence procedure results in the following coefficients:

$$\begin{aligned}
 X_{\Gamma_3}^{(\text{opt})} &\approx \mathbf{x}_{\Gamma_3}^{(\text{opt}1)} \mathbf{x}_{\Gamma_3}^{(\text{opt}1)T}; \\
 X_{\Gamma_5}^{(\text{opt})} &\approx (\mathbf{x}_{\Gamma_5}^{(\text{opt}1)} \mathbf{x}_{\Gamma_5}^{(\text{opt}1)T} + \mathbf{x}_{\Gamma_5}^{(\text{opt}2)} \mathbf{x}_{\Gamma_5}^{(\text{opt}2)T})/2; \\
 X_{\Gamma_7}^{(\text{opt})} &\approx 0; \\
 X_{\Gamma_9}^{(\text{opt})} &\approx (\mathbf{x}_{\Gamma_9}^{(\text{opt}1)} \mathbf{x}_{\Gamma_9}^{(\text{opt}1)T} + \mathbf{x}_{\Gamma_9}^{(\text{opt}2)} \mathbf{x}_{\Gamma_9}^{(\text{opt}2)T} + \mathbf{x}_{\Gamma_9}^{(\text{opt}3)} \mathbf{x}_{\Gamma_9}^{(\text{opt}3)T})/3;
 \end{aligned}$$

| IRs | Variables x | Nd1, Ir1 | Nd2, Ir2 | Nd3, Ir3 | Nd4, Ir4 |
|------------|--|------------------------|--------------------------|----------------------------|--------------------------|
| | | (0,0,0), (1/2,0,0) | (1/4,1/4,0), (3/4,1/4,0) | (0,1/4,1/4), (1/2,1/4,1/4) | (1/4,0,1/4), (3/4,0,1/4) |
| Γ_3 | $m^{(\Gamma_3, Nd)_1}, m^{(\Gamma_3, Ir)_1}$ | (1, 1, 1)/ $\sqrt{3}$ | (-1, -1, 1)/ $\sqrt{3}$ | (1, -1, -1)/ $\sqrt{3}$ | (-1, 1, -1)/ $\sqrt{3}$ |
| Γ_5 | $m^{(\Gamma_5, Nd)_1}, m^{(\Gamma_5, Ir)_1}$ | (1, -1, 0)/ $\sqrt{2}$ | (-1, 1, 0)/ $\sqrt{2}$ | (1, 1, 0)/ $\sqrt{2}$ | (-1, -1, 0)/ $\sqrt{2}$ |
| | $m^{(\Gamma_5, Nd)_2}, m^{(\Gamma_5, Ir)_2}$ | (1, 1, -2)/ $\sqrt{6}$ | (-1, -1, -2)/ $\sqrt{6}$ | (1, -1, 2)/ $\sqrt{6}$ | (-1, 1, 2)/ $\sqrt{6}$ |
| Γ_7 | $m^{(\Gamma_7, Nd)_1}, m^{(\Gamma_7, Ir)_1}$ | (0, -1, 1)/ $\sqrt{2}$ | (0, -1, -1)/ $\sqrt{2}$ | (0, 1, -1)/ $\sqrt{2}$ | (0, 1, 1)/ $\sqrt{2}$ |
| | $m^{(\Gamma_7, Nd)_2}, m^{(\Gamma_7, Ir)_2}$ | (1, 0, -1)/ $\sqrt{2}$ | (1, 0, 1)/ $\sqrt{2}$ | (-1, 0, -1)/ $\sqrt{2}$ | (-1, 0, 1)/ $\sqrt{2}$ |
| | $m^{(\Gamma_7, Nd)_3}, m^{(\Gamma_7, Ir)_3}$ | (-1, 1, 0)/ $\sqrt{2}$ | (1, -1, 0)/ $\sqrt{2}$ | (1, 1, 0)/ $\sqrt{2}$ | (-1, -1, 0)/ $\sqrt{2}$ |
| Γ_9 | $m^{(\Gamma_9, Nd)_1}, m^{(\Gamma_9, Ir)_1}$ | (1, 1, 0)/ $\sqrt{2}$ | (-1, -1, 0)/ $\sqrt{2}$ | (-1, 1, 0)/ $\sqrt{2}$ | (1, -1, 0)/ $\sqrt{2}$ |
| | $m^{(\Gamma_9, Nd)_2}, m^{(\Gamma_9, Ir)_2}$ | (0, 1, 1)/ $\sqrt{2}$ | (0, 1, -1)/ $\sqrt{2}$ | (0, -1, -1)/ $\sqrt{2}$ | (0, -1, 1)/ $\sqrt{2}$ |
| | $m^{(\Gamma_9, Nd)_3}, m^{(\Gamma_9, Ir)_3}$ | (1, 0, 1)/ $\sqrt{2}$ | (1, 0, -1)/ $\sqrt{2}$ | (-1, 0, 1)/ $\sqrt{2}$ | (-1, 0, -1)/ $\sqrt{2}$ |
| | — | (1, 0, 0) | (1, 0, 0) | (1, 0, 0) | (1, 0, 0) |
| | — | (0, 1, 0) | (0, 1, 0) | (0, 1, 0) | (0, 1, 0) |
| | — | (0, 0, 1) | (0, 0, 1) | (0, 0, 1) | (0, 0, 1) |

Table 2. Basis vectors of the magnetic structures represented by the Γ_3 , Γ_5 , Γ_7 and Γ_9 IRs^{18,35}. The symbol – in the Γ_9 IR indicates that the ferromagnetic basis vectors are precluded.

and

$$\begin{aligned}
 \mathbf{x}_{\Gamma_3}^{(\text{opt})} &= (-1.20, 0.19); \\
 \mathbf{x}_{\Gamma_5}^{(\text{opt1})} &= (0.55, 0., 0.48, 0.), \quad \mathbf{x}_{\Gamma_5}^{(\text{opt2})} = (0., 0.55, 0., 0.48); \\
 \mathbf{x}_{\Gamma_7}^{(\text{opt})} &= (0., 0., 0., 0., 0., 0.); \\
 \mathbf{x}_{\Gamma_9}^{(\text{opt1})} &= (0.55, 0., 0., -0.52, 0., 0.), \quad \mathbf{x}_{\Gamma_9}^{(\text{opt2})} = (0., 0.55, 0., 0., -0.52, 0.), \\
 \mathbf{x}_{\Gamma_9}^{(\text{opt3})} &= (0., 0., 0.55, 0., 0., -0.52);
 \end{aligned}$$

where the values of \mathbf{x} are expressed the μ_B units, and the negative sign indicates the nearest ferromagnetic Nd–Ir correlation. While a single optimum solution is determined for representation Γ_3 , multiple solutions are obtained for Γ_5 and Γ_9 , respectively, in accordance with the rank values of $X_{\Gamma_5}^{(\text{opt})}$ and $X_{\Gamma_9}^{(\text{opt})}$, which indicate the existence of an infinite number of solutions with the same objective functions $\mathbf{x}_{\Gamma_5}^{(\text{opt})} = \cos\theta\mathbf{x}_{\Gamma_5}^{(\text{opt1})} + \sin\theta\mathbf{x}_{\Gamma_5}^{(\text{opt2})}$ and $\mathbf{x}_{\Gamma_9}^{(\text{opt})} = \cos\theta\mathbf{x}_{\Gamma_9}^{(\text{opt1})} + \sin\theta\cos\phi\mathbf{x}_{\Gamma_9}^{(\text{opt2})} + \sin\theta\sin\phi\mathbf{x}_{\Gamma_9}^{(\text{opt3})}$, where θ and ϕ are arbitrary. Without SDR, it is difficult to find the optimum solutions for this type of problems and prove that better solutions do not exist. Furthermore, the zero magnitude of $\mathbf{x}_{\Gamma_7}^{(\text{opt})}$ is obtained for representation Γ_7 . Indeed, when \mathbf{x}_{Γ_7} values are finite (non-zero), the $I_{\text{mag,cal}}$ values for $I_{\text{mag,obs}} = 0$ indices increase more rapidly than those for $I_{\text{mag,obs}} \neq 0$ indices. Thus, the SDR method automatically overcomes these issues.

(2) The obtained indicator values for representations Γ_3 , Γ_5 , Γ_7 and Γ_9 are as follows.

- The corresponding duality gaps determined by the SDP solver are equal to $\Delta f = 2.1 \times 10^{-7}, 1.4 \times 10^{-6}, 3.1 \times 10^{-6}$ and 8.0×10^{-7} , respectively. Their magnitudes are close to zero, indicating that the convergence to the global optimum is achieved.
- The minimized objective function $f^{(\text{gl})} \stackrel{\text{def}}{=} \sum_{k=1}^N |I_{\text{mag,obs}}(Q_k) - I_{\text{mag,cal}}(Q_k)| / \text{Err}[I_{\text{mag,obs}}(Q_k)] = 4.5, 19, 32$ and 27, and the more familiar R -factor, $R_{\text{Bragg}} \stackrel{\text{def}}{=} \left(\sum_{k=1}^N |I_{\text{mag,obs}}(Q_k) - I_{\text{mag,cal}}(Q_k)| \right) / \left(\sum_{k=1}^N I_{\text{mag,obs}}(Q_k) \right) = 0.13, 0.63, 1.0$ and 0.81, respectively. These results show that the smallest values are obtained for representation Γ_3 .
- The goodness of the fit $\chi^2 \stackrel{\text{def}}{=} \left(\sum_{k=1}^N |I_{\text{mag,obs}}(Q_k) - I_{\text{mag,cal}}(Q_k)|^2 / \text{Err}[I_{\text{mag,obs}}(Q_k)]^2 \right) / (N - n_{\Gamma}) = 2.6, 14, 25$ and 20, and the related statistical parameter $f^{(\text{gl})} / (N - n_{\Gamma}) = 0.75, 4.8, 16$ and 14, respectively. The value closest to the expected value (1 for χ^2 ; $\sqrt{2/\pi} \approx 0.798$ for the latter parameter) is obtained for Γ_3 .

All these facts suggest that Γ_3 represents the best solution, whereas representations Γ_5 , Γ_7 and Γ_9 are excluded for the first time. For clarity, the values of $I_{\text{mag,cal}}$ are listed in Table 2 and also shown in Fig. 3. The magnitude of $I_{\text{mag,cal-}\Gamma_3}$ matches $I_{\text{mag,obs}}$ very well, whereas the globally optimal $I_{\text{mag,cal-}\Gamma_5}$, $I_{\text{mag,cal-}\Gamma_7}$ and $I_{\text{mag,cal-}\Gamma_9}$ parameters substantially differ from the corresponding $I_{\text{mag,obs}}$ values.

After proving mathematically the uniqueness of representation Γ_3 , the refined values $m_{\text{Nd}} = -1.22(5)\mu_B$ and $m_{\text{Ir}} = 0.14(5)\mu_B$ are obtained using the $\mathbf{x}_{\Gamma_3}^{(\text{opt})}$ values as the initial parameters in the normal least-squares method. These results are comparable with the reported values of $m_{\text{Nd}} = -1.27(1)\mu_B$ and $m_{\text{Ir}} = 0.34(1)\mu_B$ ³⁴.

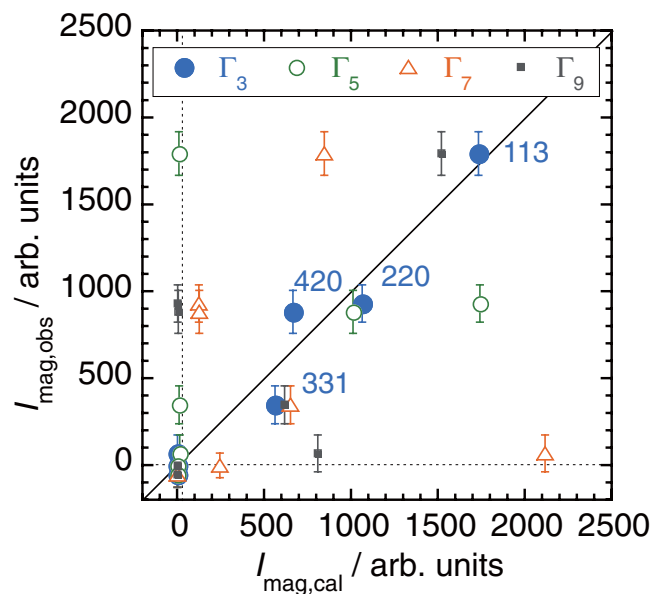


Figure 3. Comparison of the $I_{\text{mag,obs}}$ (1.4 K) and $I_{\text{mag,cal}}$ values. The diagonal straight line represents the condition $I_{\text{mag,obs}} = I_{\text{mag,cal}}$.

Discussion

Representation Γ_9 (the only IR containing ferromagnetic basis vectors³⁵) is rejected as the optimal solution despite the existence of weak ferromagnetism²⁹. The observed inconsistency suggests that this ferromagnetism is symmetrically decoupled from the bulk magnetic structure (for example, as a surface or interface-protected property). In fact, by performing careful measurements of the macroscopic magnetization and electrical resistivity of isomorphous $\text{Cd}_2\text{Os}_2\text{O}_7$, it was found that the surface ferromagnetism coupled with novel spin-polarized conductivity emerged on the walls between the all-in all-out and all-out all-in antiferromagnetic domains³⁶. The macroscopic observation is consistent with the findings of this study verified both microscopically and mathematically, indicating their potential applicability in domain wall spin electronics.

We discuss the expected application scope of the SDR method. After determining the list of $(h_{\text{mag}}, k_{\text{mag}}, I_{\text{mag}}, I_{\text{mag,obs}})$ values, the described SDR method can be used to find the corresponding magnetic structures as the global solutions. First, the configurations with $\mathbf{k}_{\text{mag}} = (0, 0, 0)$ are considered, indicating their high potential applicability in various fields (including magnet materials). Second, this method is not restricted to polarized neutron diffraction experiments, but can be also used in studies involving unpolarized neutrons when the magnetic structure is characterized by $\mathbf{k}_{\text{mag}} \neq (0, 0, 0)$ or $\mathbf{k}_{\text{mag}} = (0, 0, 0)$ with detectable magnetic moment. Both the magnetic and crystallographic structures can be simultaneously refined by the normal least-squares method, in which the obtained SDR solutions are utilized as the initial values of the magnetic structural parameters. Third, the SDR technique is able to easily process thousands of independent variables. Therefore, magnetic structures of arbitrary types can be theoretically determined using the advanced diffractometers that provide a relatively large number of reflection points (even for the target materials with complex compositions).

The diffraction intensities are not represented by quadratic functions of the atomic positions r_j ; hence, the SDR technique seems to be inapplicable for determining the values of r_j (crystal structure). However, the neutron and X-ray diffraction intensities are represented by those of the nuclear and electron densities (generalized crystal structure), respectively. Likewise, a magnetic structure is also generalized to the magnetic moment density. Thus, the SDR technique is expected to enable analysing the global solutions of the generalized structures together with the aforementioned high-volume processing ability, such as protonic/ionic distributions in the conductors and electronic spin-orbital distributions.

Materials and Methods

Calculations. The system of quadratic equations was solved using the SDP solver SDPA³⁷. To find the global optima of SDP problems, interior point methods were efficiently used³⁸.

Experiments. The polarized neutron elastic scattering experiments were performed using the HB1 thermal neutron three-axis spectrometer located at the High Flux Isotope Reactor (HFIR) of the Oak Ridge National Laboratory (ORNL). Heusler alloy 111 reflection crystals were utilized as the monochromator and analyser. The flipping ratio $R = 10$ was obtained using the nuclear 222 reflection at a paramagnetic temperature of 40 K corresponding to the beam polarization $P = 0.82$. The polarization vector was set parallel to the scattering vector ($P//Q$). The incident energy of neutrons was $E_i = 13.5$ meV. The horizontal collimator sequence was $48'(\text{open})-80'-80'-240'$. A pyrolytic graphite Bragg-reflection filter was used to efficiently eliminate the contamination caused by higher-order wavelengths.

A powder $\text{Nd}_2\text{Ir}_2\text{O}_7$ sample was synthesized by a solid-state reaction method inside a quartz tube. About 4.8 g of the sample was wrapped in thin aluminium foil and shaped to a hollow cylinder with a thickness of 0.8 mm and diameter of 20 mm to mitigate the effect of the strong neutron absorption of Ir nuclei. The cylinder was stored in an aluminium container filled with He gas and placed under the cold heads of a He-closed-cycle (Displex) or liquid-He-type (Orange) cryostat.

References

- Shull, C. G., Strauser, W. A. & Wollan, E. O. Neutron diffraction by paramagnetic and antiferromagnetic substances. *Phys. Rev.* **83**, 333 (1951).
- Booth, A. D. Application of the method of steepest descents to X-Ray structure analysis. *Nature* **160**, 196 (1947).
- Cochran, W. The Fourier method of crystal structure analysis. *Nature* **161**, 765 (1948).
- Kimura, T. *et al.* Magnetic control of ferroelectric polarization. *Nature* **426**, 55 (2003).
- Vaknin, D. *et al.* Antiferromagnetism in $\text{La}_2\text{CuO}_{4-y}$. *Phys. Rev. Lett.* **58**, 2802–2805 (1987).
- Tranquada, J. M. *et al.* Neutron-diffraction determination of antiferromagnetic structure of Cu ions in $\text{YBa}_2\text{Cu}_3\text{O}_{6+x}$ with $x = 0.0$ and 0.15 . *Phys. Rev. Lett.* **60**, 156 (1988).
- de la Cruz, C. *et al.* Magnetic order close to superconductivity in the iron-based layered $\text{LaO}_{1-x}\text{F}_x\text{FeAs}$ systems. *Nature* **453**, 899 (2008).
- Tokura, Y., Kawasaki, M. & Nagaosa, N. Emergent functions of quantum materials. *Nat. Phys.* **13**, 1056 (2017).
- Tsujimoto, Y. *et al.* Infinite-layer iron oxide with a square-planar coordination. *Nature* **450**, 1062 (2007).
- Ovsyannikov, S. V. *et al.* Charge-ordering transition in iron oxide Fe_4O_5 involving competing dimer and trimer formation. *Nat. Chem.* **8**, 501 (2016).
- Michel, F. M. *et al.* Ordered ferrimagnetic form of ferrihydrite reveals links among structure, composition, and magnetism. *PNAS* **107**, 2787 (2010).
- Izmaylov, Y. A., Naish, V. E. & Ozerov, R. R. *Neutron Diffraction of Magnetic Materials* (Consultants Bureau, New York, 1991).
- Kovalev, O. Representations of the Crystallographic Space Groups (Gordon and Breach, Switzerland, 1993).
- Bertaut, E. F. Representation Analysis of Magnetic Structures. *Acta Cryst.* **A24**, 217 (1968).
- For example, Torii, S., Yonemura, M., Ishikawa, Y., Miao, P., Tomiyasu, R., Satoh, S., Noda, Y. & Kamiyama, T. Improvement of Instrument Devices for Super High Resolution Powder Diffractometer at J-PARC. *J. Phys.: Conf. Ser.* **502**, 12052 (2014).
- Willis, B. T. M. & Carlile, C. J. *Experimental Neutron Scattering* (Oxford University Press, 2017).
- Lovesey, S. W. *Theory of Neutron Scattering from Condensed Matter* (Oxford University Press, 1984).
- Wills, A. S. A new protocol for the determination of magnetic structures using simulated annealing and representational analysis (SARAh). *Physica B (Amsterdam, Neth.)* **276–278**, 680 (2000).
- Rodríguez-Carvajal, J. Recent advances in magnetic structure determination neutron powder diffraction. *Physica B (Amsterdam, Neth.)* **192**, 55 (1993).
- McGreevy, R. L. & Pusztai, L. Reverse Monte Carlo Simulation: A New Technique for the Determination of Disordered Structures. *Journal Molecular Simulation* **1**, 359 (1988).
- Harris, K. D. M., Tremayne, M., Lightfoot, P. & Bruce, P. G. Crystal Structure Determination from Powder Diffraction Data by Monte Carlo Methods. *J. Am. Chem. Soc.* **116**, 3543 (1994).
- Shankland, K., David, W. I. F. & Csoka, T. Crystal structure determination from powder diffraction data by the application of a genetic algorithm. *Zeitschrift für Kristallographie* **212**, 550 (1997).
- Harris, K. D. M., Johnston, R. L. & Kariuki, B. M. The Genetic Algorithm: Foundations and Applications in Structure Solution from Powder Diffraction Data. *Acta Crystallographica A* **54**, 632 (1998).
- Blekherman, G. & Parrilo, P. A., Ed. Thomas, R. R. Semidefinite Optimization and Convex Algebraic Geometry in *MOS-SIAM Series on Optimization*. (Society for Industrial and Applied Mathematics and Mathematical Optimization Society, Philadelphia, 2013).
- Candès, E. J., Strohmer, T. & Vershynski, V. PhaseLift: Exact and Stable Signal Recovery from Magnitude Measurements via Convex Programming. *Commun. Pure and Appl. Math.* **66**, 1241 (2013).
- Oishi-Tomiyasu, R. Application of convex optimization to identification of atomic species from diffraction patterns. *Powder Diffraction J.* **32**(S1), S179 (2017).
- Pesin, D. & Balents, L. Mott physics and band topology in materials with strong spin–orbit interaction. *Nat. Phys.* **6**, 376 (2010).
- Matsuhira, K. *et al.* Metal–Insulator Transition in Pyrochlore Iridates $\text{Ln}_2\text{Ir}_2\text{O}_7$ ($\text{Ln} = \text{Nd}, \text{Sm}, \text{and Eu}$). *J. Phys. Soc. Jpn.* **76**, 043706 (2007).
- Matsuhira, K., Wakeshima, M., Hinatsu, Y. & Takagi, S. Metal–Insulator Transitions in Pyrochlore Oxides $\text{Ln}_2\text{Ir}_2\text{O}_7$. *J. Phys. Soc. Jpn.* **80**, 094701 (2011).
- Yamaji, Y. & Imada, M. Metallic Interface Emerging at Magnetic Domain Wall of Antiferromagnetic Insulator: Fate of Extinct Weyl Electrons. *Phys. Rev. X* **4**, 021035 (2014).
- Tian, Z. *et al.* Field-induced quantum metal–insulator transition in the pyrochlore iridate $\text{Nd}_2\text{Ir}_2\text{O}_7$. *Nat. Phys.* **12**, 134 (2015).
- Wan, X., Turner, A. M. & Vishwanath, A. & Savrasov, S. Y. Topological Semimetal and Fermi–Arc Surface States in the Electronic Structure of Pyrochlore Iridates. *Phys. Rev. B* **83**, 205101 (2011).
- Tomiyasu, K. *et al.* Emergence of Magnetic Long-range Order in Frustrated Pyrochlore $\text{Nd}_2\text{Ir}_2\text{O}_7$ with Metal–Insulator Transition. *J. Phys. Soc. Jpn.* **81**, 034709 (2012).
- Guo, H., Ritter, C. & Komarek, A. C. Direct determination of the spin structure of $\text{Nd}_2\text{Ir}_2\text{O}_7$ by means of neutron diffraction. *Phys. Rev. B* **94**, 161102(R) (2016).
- Wills, A. S. *et al.* Magnetic ordering in $\text{Gd}_2\text{Sn}_2\text{O}_7$: the archetypal Heisenberg pyrochlore antiferromagnet. *J. Phys. Condens. Matter Lett.* **18**, L37 (2006).
- Hirose, H. T., Yamaura, J. & Hiroi, Z. Robust ferromagnetism carried by antiferromagnetic domain walls. *Sci. Rep.* **7**, 42440.
- Yamashita, M. *et al.* A high-performance software package for semidefinite programs: SDPA 7. *Research Report B-460* (Dept. of Mathematical and Computing Science, Tokyo Institute of Technology, Tokyo, Japan) (2010).
- Vandenbergh, L. & Boyd, S. Semidefinite Programming. *SIAM Review* **38**, 49 (1996).

Acknowledgements

Neutron diffraction experiments were conducted using the High Flux Isotope Reactor, a user facility of the DOE Office of Science operated by the Oak Ridge National Laboratory (USA). This study was partially supported by the U.S.-Japan Cooperative Program on Neutron Scattering. This study was financially supported by the MEXT/JSPS KAKENHI (grant Nos JP18K03503, JP17H06137 and JP15H03692), JST PRESTO (grant No. JPMJPR14E6), Japan-US program administrated by ISSP at the University of Tokyo and FRIS program for the creation of interdisciplinary research at the Tohoku University.

Author Contributions

K.T. conceived and conducted this study. R.O.-T. performed the mathematical optimization. K.M. synthesized the sample. K.T. and M.M. performed the neutron diffraction experiments. K.T. and R.O.-T. analysed the data. K.T. and R.O.-T. wrote the manuscript based on the feedback provided by all authors.

Additional Information

Supplementary information accompanies this paper at <https://doi.org/10.1038/s41598-018-34443-2>.

Competing Interests: The authors declare no competing interests.

Publisher's note: Springer Nature remains neutral with regard to jurisdictional claims in published maps and institutional affiliations.



Open Access This article is licensed under a Creative Commons Attribution 4.0 International License, which permits use, sharing, adaptation, distribution and reproduction in any medium or format, as long as you give appropriate credit to the original author(s) and the source, provide a link to the Creative Commons license, and indicate if changes were made. The images or other third party material in this article are included in the article's Creative Commons license, unless indicated otherwise in a credit line to the material. If material is not included in the article's Creative Commons license and your intended use is not permitted by statutory regulation or exceeds the permitted use, you will need to obtain permission directly from the copyright holder. To view a copy of this license, visit <http://creativecommons.org/licenses/by/4.0/>.

© The Author(s) 2018